

RESEARCH ARTICLE | MARCH 31 2025

Generation of high and bidirectional out-of-plane spin-orbit torque through vertical magnetization gradient

Tianli Jin ; Yuliang Zhu ; Shaomin Li ; Bo Zhang; Funan Tan ; Gerard Joseph Lim ; Jiangwei Cao ; Kaiming Cai ; Wen Siang Lew  

 Check for updates

Appl. Phys. Lett. 126, 132401 (2025)

<https://doi.org/10.1063/5.0251658>



View Online



Export Citation

Articles You May Be Interested In

Vectorial observation of the spin Seebeck effect in epitaxial NiFe₂O₄ thin films with various magnetic anisotropy contributions

Appl. Phys. Lett. (June 2019)

Spin-flop process identified in heteroepitaxial rare-earth films of Er and Ho

Appl. Phys. Lett. (April 2024)

Intrinsic spin Hall effect in oxidized platinum/magnetic oxide heterostructure

Appl. Phys. Lett. (September 2022)

02 May 2025 15:07:24



BLUE FORS

Accelerate your research.
Scale up your experiments with increased cooling power and a new side-loading LD system.

[Discover the latest advances in cooling](#)

Generation of high and bidirectional out-of-plane spin-orbit torque through vertical magnetization gradient

Cite as: Appl. Phys. Lett. **126**, 132401 (2025); doi: [10.1063/5.0251658](https://doi.org/10.1063/5.0251658)

Submitted: 4 December 2024 · Accepted: 19 March 2025 ·

Published Online: 31 March 2025



View Online



Export Citation



CrossMark

Tianli Jin,^{1,2,a)} Yuliang Zhu,³ Shaomin Li,^{1,4} Bo Zhang,^{1,5} Funan Tan,¹ Gerard Joseph Lim,¹ Jiangwei Cao,⁵ Kaiming Cai,³ and Wen Siang Lew^{1,a)}

AFFILIATIONS

¹School of Physical and Mathematical Sciences, Nanyang Technological University, 21 Nanyang Link, 637371 Singapore

²School of Integrated Circuits, Huazhong University of Science and Technology, Wuhan 430074, China

³School of Physics, Huazhong University of Science and Technology, Wuhan 430074, China

⁴Department of Electrical Engineering, School of Internet of Things (IoTs), Institute of Advanced Technology, Jiangnan University, Wuxi 214122, China

⁵School of Physical Science and Technology, Lanzhou University, Lanzhou 730000, China

^{a)}Authors to whom correspondence should be addressed: tianli.jin@ntu.edu.sg and wensiang@ntu.edu.sg

ABSTRACT

High efficiency and out-of-plane spin-orbit torque (OOP-SOT) driven magnetization switching is essential for developing spin-based memory and logic devices. In this study, we report the generation of a large charge-to-spin conversion and bidirectional OOP-SOT by engineering a vertical magnetization gradient within a Co/Ho multilayer system. Exploiting the antiferromagnetic coupling between Co and Ho, the magnetization gradient up to 16.8 (emu/cm⁻³)/nm was achieved by gradually varying the Ho layer thickness from 0.4 to 0.9 nm. The presence of the OOP-SOT was confirmed through Hall resistance-field loop shift measurements, which has been attributed to the broken symmetry in spin current reflection and transmission in the Co/Ho multilayer with vertical magnetic property gradients. Additionally, the effective field of the OOP-SOT is strongly correlated with the direction of the magnetization gradient, measured to be around +0.7 and -2.5 Oe/mA for the positive and negative magnetization gradients, respectively. Furthermore, the largest SOT in the Co/Ho multilayer with a negative gradient was observed compared to the positive gradient and uniform Co/Ho multilayer structures. The enhanced SOT is attributed to the bulk Rashba field generated by the gradient structure, along with increased spin polarization. The results demonstrated here provide a promising approach for utilizing magnetization gradients for the development of efficient, current-driven spin-based storage and logic devices.

Published under an exclusive license by AIP Publishing: <https://doi.org/10.1063/5.0251658>

The exploration of suitable materials and structures is continuously progressing to achieve high-density, efficient, and purely current-driven spin-based storage and logic devices.^{1,2} For high-density memory applications, information is typically encoded in magnets with perpendicular magnetic anisotropy (PMA).³ For memory and logic operations, spin-orbit torque (SOT) has emerged as a promising approach for achieving efficient and rapid magnetization control. However, conventional SOT with in-plane polarized spin orientation, cannot realize deterministic switching in PMA systems without an external magnetic field.^{4,5} To address this limitation, out-of-plane SOT (OOP-SOT), referred to as unconventional SOT with out-of-plane polarized spin orientation, has gained attention.⁶⁻⁹ Achieving the unconventional SOT, along with reducing switching current density, is

essential for the technological realization of spin-based memory and logic devices.

Previous research has explored the materials with broken inversion symmetry to generate spin polarization σ_z along the OOP direction.⁶⁻¹¹ In these systems, the spin current with OOP spin polarization, which is parallel to the spin-current direction, can drive the deterministic magnetization switching of a PMA magnetic layer. Experimentally validated materials include L₁₁-ordered CuPt,⁶ van der Waals material WTe₂,^{7,8} Weyl semimetal TaIrTe₄,⁹ and some antiferromagnetic materials (AFM).^{10,11} These materials require epitaxial growth, high-temperature annealing, or mechanical exfoliation, which is not ideal for wafer-level application, and they typically lack high charge-to-spin current conversion efficiency. Simultaneously, to

achieve low power consumption, materials with strong spin-orbit coupling (SOC) generating large in-plane spin polarization are continuously explored. To achieve both high charge-to-spin conversion and OOP-SOT, research has focused on bulk SOT systems. In particular, Jinnai *et al.* and Chen *et al.* reported a twofold enhancement of SOT efficiency using thick ferromagnetic layers, such as Pt/Co multilayers with varying stacking numbers.^{12,13} This enhancement is attributed to the contributions of bulk SOC and the breaking of interface symmetry. Moreover, Zheng *et al.* demonstrated the generation of antisymmetric Dzyaloshinskii–Moriya interaction (DMI) in a bulk CoTb structure with vertical composition gradient, which enables chiral symmetry breaking of the DMI and leads to the deterministic SOT switching.¹⁴

In this study, to realize high charge-to-spin conversion and unconventional SOT, we report the design of a vertical magnetization gradient using a Co/Ho multilayer system. We demonstrated bidirectional OOP-SOT and achieved high SOT efficiency in this gradient system. The vertical magnetization gradient was realized by tuning Co and Ho thickness, resulting in a gradual change in saturation magnetization (M_s). By varying the Ho thickness from 0.4 to 0.9 nm, we achieved the M_s gradient up to 16.8 (emu/cm³)/nm. The effective field of the OOP-SOT was measured to be around +0.7 Oe/mA for the positive gradient and -2.5 Oe/mA for the negative gradient. Furthermore, the large SOT efficiency was attained in the Co/Ho multilayer sample with a negative M_s gradient, which can be attributed to the bulk Rashba field generated by the gradient structure. This enhancement is further supported by increased spin polarization (σ) with the sum of the spin Hall effect (σ_{SHE}) and the Rashba effect (σ_{R}).

The Co/Ho multilayers were grown using magnetron sputtering under a base pressure of 4×10^{-8} Torr and a working Ar pressure of

3 mTorr. The thin film properties were characterized using a Lakeshore vibrating sample magnetometer (VSM). Anomalous Hall resistance (R_{xy}) was measured at a current density of 1×10^{10} A/m² with a sweeping OOP magnetic field (H_z). For current-induced magnetization switching, 500 μ s current pulses were generated using a Keithley 6221 source, and the corresponding voltages were recorded using a Keithley 2182 nanovoltmeter. The OOP-SOT was estimated by measuring the shift in the R_{xy} - H_z loops while varying the in-plane DC currents. SOT efficiency was characterized using harmonic Hall voltage measurements.

The structure with M_s vertical gradient was achieved by alternately depositing Ho and Co layers, with an increment (or decrement) thickness of the Ho layer. The investigated stacks consist of Ru (2 nm)/Pt (4 nm)/(Co/Ho)₅/Ru (2 nm), as illustrated in Fig. 1(a). The subscript 5 represents the number of repeated sequences of the Co/Ho multilayer. First, the Co/Ho multilayer structure with a Co layer thickness of 0.6 nm and varying Ho thickness was measured to investigate the magnetic properties. Figure 1(b) shows the hysteresis loops of the (Co/Ho)₅ with varying Ho thickness from 0.3 to 1.1 nm. The square loops observed in all the films indicate that they exhibit PMA. With $t_{\text{Ho}} = 0.3$ nm, the switching loop along H_z requires a large field to be fully magnetized, which is due to the strong coupling between Ho and Co layers.¹⁵ With further increasing Ho thickness, the switching field gradually reduces and reaches saturation. Figure 1(c) displays the variations in M_s for different Ho thicknesses. The change in M_s can be attributed to the intermixing between the Co and Ho layers, as well as the enhanced antiferromagnetic coupling at the Co/Ho interface with increasing Ho thickness.^{16,17} By varying the Ho layer thickness within the stack structure, we fabricated structures with M_s gradient, either a

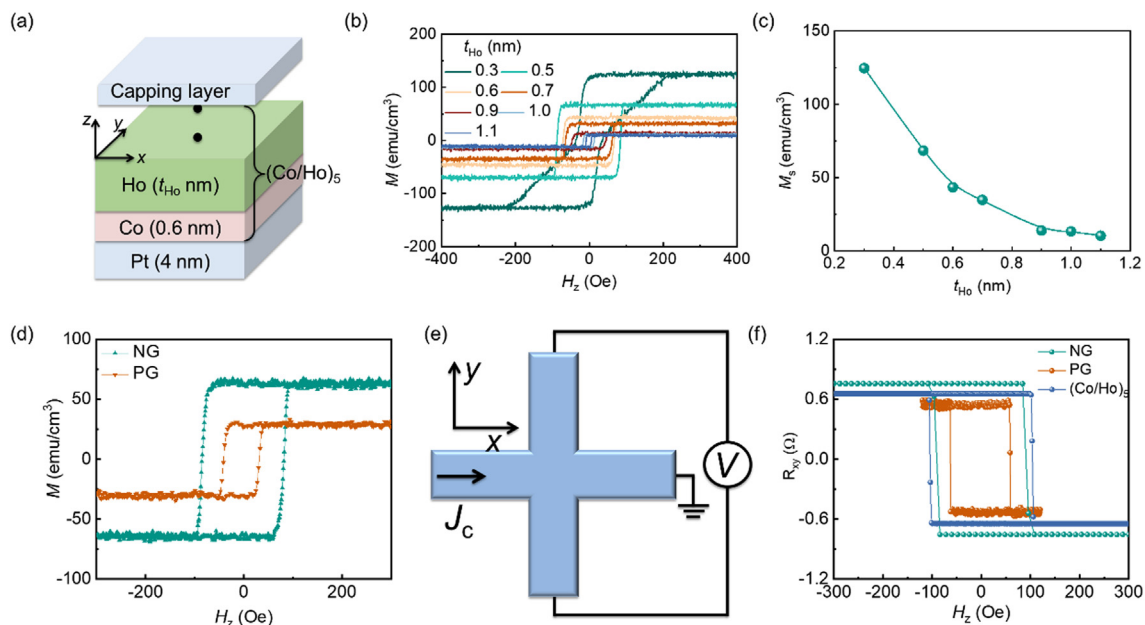


FIG. 1. The magnetic properties of the control and gradient samples. (a) Schematic diagram of designing the Co/Ho multilayer structure. (b) Hysteresis loops of (Co/Ho)₅ multilayer samples with Co thickness of 0.6 nm and varying Ho thickness from 0.3 to 1.1 nm. (c) Summary of saturation magnetization (M_s) in Co/Ho multilayer samples with different Ho thicknesses. (d) Hysteresis loops of the gradient samples. NG indicates M_s decreased from bottom to top, and PG indicates M_s increased from bottom to top. (e) Geometric illustration of harmonic Hall voltage measurement. (f) Hall resistance R_{xy} with out-of-plane magnetic field H_z for the NG, PG, and (Co/Ho)₅ samples.

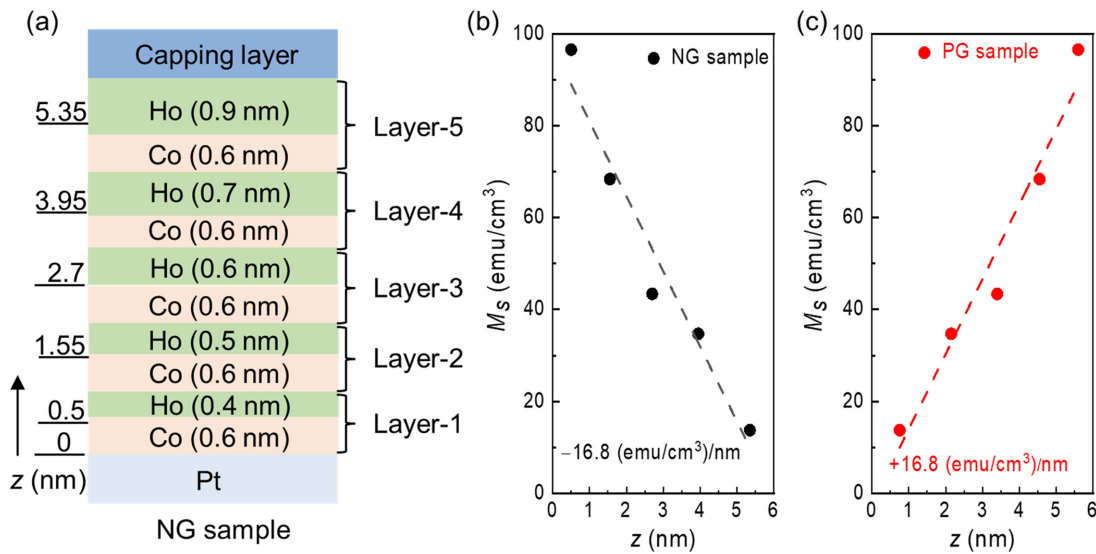


FIG. 2. The schematic diagram of the NG sample and M_s variation along the z -direction for the NG and PG samples. (a) Schematic representation of the NG sample, where adjacent Co and Ho layers are considered as a single unit, labeled as layers (1–5). (b) and (c) The M_s variation along the z -distance for the NG and PG samples, respectively. The slope of the fitted line represents the magnetization gradient.

negative gradient (NG) or a positive gradient (PG). For the NG sample, the Ho thickness increases from 0.4 to 0.9 nm from the bottom to the top. For the PG sample, the Ho thickness exhibited the opposite gradient, decreasing from 0.9 nm at the bottom to 0.4 nm at the top. M_s and coercivity H_c are sensitive to the direction of the Ho gradient. M_s of the NG sample exhibits a significantly higher value at 75 emu/cm^3 , in contrast to the PG sample, which shows a lower value of 27 emu/cm^3 , as depicted in Fig. 1(d). Lower H_c is also observed in the PG sample. The sensitivity of those gradient samples is attributed to the PMA arising from its interfacial energy, which also provides tunability for designing various gradient structures.

To investigate the current-driven magnetization dynamics, the Hall bar devices have been fabricated with dimensions of $5 \mu\text{m}$ width and $60 \mu\text{m}$ length, as shown in Fig. 1(e). The control sample (Co/Ho)₅ with a uniform M_s was also prepared for comparison. Here, the thickness of Co and Ho is 0.6 and 0.5 nm, respectively. Hall resistance measurement was conducted for all the samples. The applied current density J_c is $1 \times 10^{10} \text{ A/m}^2$ for R_{xy} detection. R_{xy} change with H_z is presented in Fig. 1(f). A higher H_c in Hall bar devices for PG and NG samples compared to the as-deposited films was observed. For the PG sample, H_c increases to 61 Oe, while the thin film shows a low H_c of 36 Oe. Similarly, for the NG sample, H_c slightly increases from 83 to 92 Oe. This can be attributed to the interlayer mixing effect during the device fabrication process involving 115°C hot-plate baking. The variation in H_c for those samples with Hall bar shape will be considered in the following discussions when we compare the critical current density and estimate the energy efficiency for the current-driven magnetization switching.

The M_s gradient $\nabla_z M_s$ is defined as $\Delta M_s(z)/\Delta z$, where $\Delta M_s(z)$ represents the saturation magnetization M_s variation along the z -axis. To estimate this gradient, the adjacent Co/Ho bilayer was considered as a single unit, referred to as layers (1–5) and as illustrated in Fig. 2(a). The values of M_s for layers (1–5) are taken from the

individual film stacks, as presented in Fig. 1(c). The slopes of M_s vs thickness for the NG and PG samples are extracted from a linear fitting, as shown in Figs. 2(b) and 2(c), respectively. From this analysis, the estimated magnetization gradients are $\pm 16.8 \text{ (emu/cm}^3\text{)}/\text{nm}$ for the NG and PG samples, respectively. Experiments were conducted to measure the SOT-driven magnetization switching in the NG, PG, and (Co/Ho)₅ samples under varying external in-plane fields, as shown in Figs. 3(a)–3(c). The results demonstrated typical SOT-driven magnetization switching with the H_x larger than 120 Oe, and the reversed switching chirality indicates SOT switching behavior when the H_x direction is reversed. Additionally, we observed that the in-plane field assisted magnetization switching responds to the gradient direction. For the NG sample, clear switching was observed with $H_x = -60 \text{ Oe}$, but no switching was observed with $H_x = +60 \text{ Oe}$. Conversely, there is no clear switching with $H_x = -60 \text{ Oe}$ for the PG sample, and with $H_x = +60 \text{ Oe}$, almost 60% magnetization switching has been observed. For the control sample (Co/Ho)₅ without M_s gradient, it shows the symmetrical switching under $H_x = \pm 60 \text{ Oe}$ during the switching polarity reversal. The asymmetric position of H_x in the NG and PG samples originates from the gradient structure, and it is determined by the DMI energy, given by $\Delta E_{\text{DMI}} \propto D \nabla_z M_s$.¹⁸ The direction of H_x is determined by the orientation of $\nabla_z M_s$, and the magnitude of H_x is dictated by the combined effect of the DMI constant (D) and the strength of $\nabla_z M_s$. Figure 3(d) summarizes the switching ratio as a function of H_x . The control sample exhibited symmetrical switching behavior with varying H_x . However, the NG and PG samples displayed opposite switching ratios, revealing a hidden effective field dependent on the M_s gradient direction. We propose that the effective field originates from the vertical gradient composition of M_s . However, we have not observed an obvious deterministic SOT switching in the absence of H_x , which is attributed to the weak gradient DMI effect in the Co/Ho system.^{18–22}

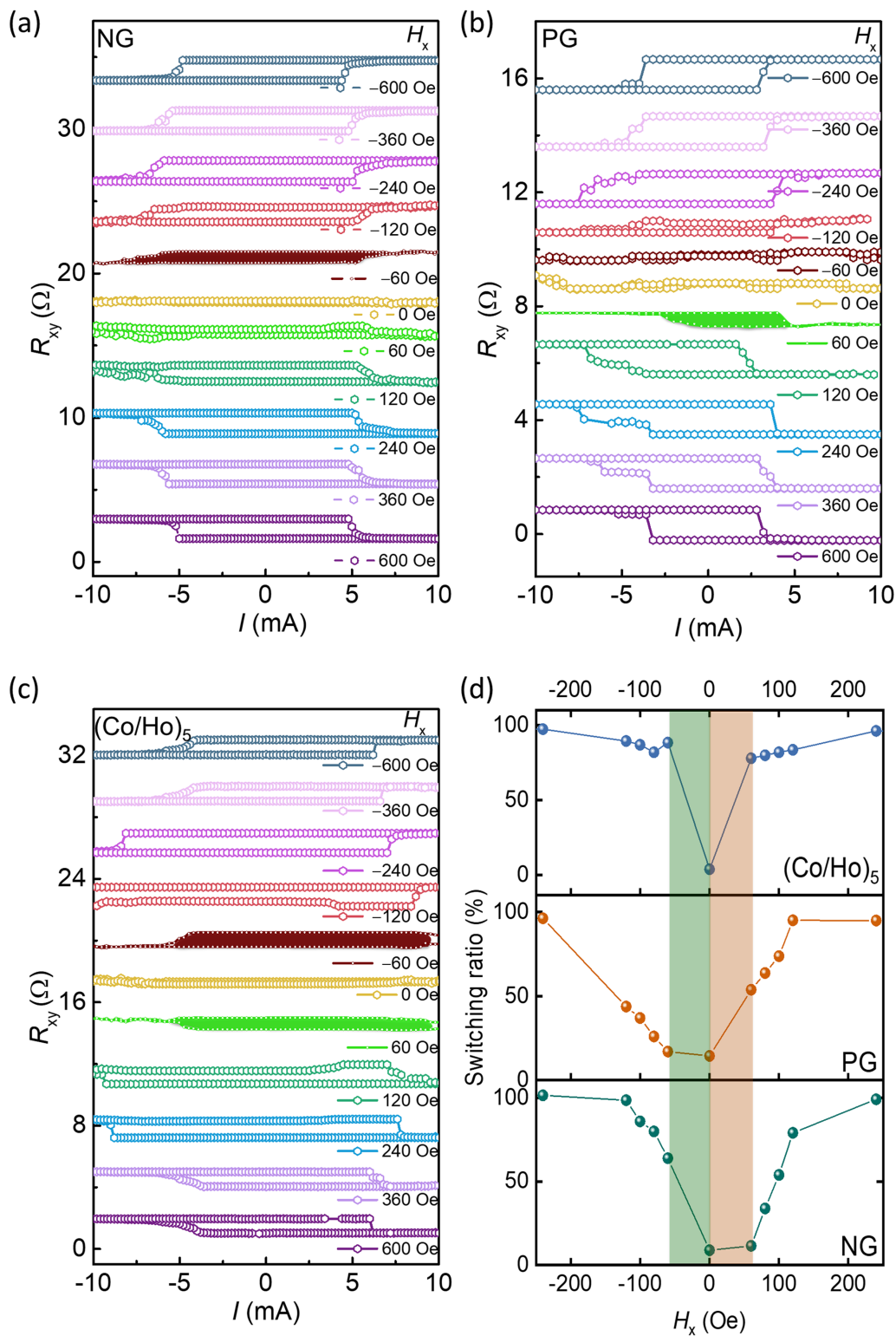


FIG. 3. Asymmetric switching behavior driven by current. (a)–(c) Current-induced magnetization switching in the NG, PG, and (Co/Ho)₅ samples. (d) Comparison of switching ratio with different in-plane fields for the NG, PG, and (Co/Ho)₅ samples.

Additionally, we noted the switching current in the NG sample is smaller compared to the (Co/Ho)₅ sample. As shown in Figs. 4(a)–4(c), the critical switching current J_{sw} is 5.68, 4.8, and 6.79 mA for the NG, PG, and (Co/Ho)₅ samples, respectively. When accounting for the variation in H_c , the J_{sw}/H_c ratio is 0.62 for the NG sample and 0.79 for the PG sample. The NG sample demonstrated more efficient magnetization switching, which can be attributed to its high SOT efficiency. As depicted in Fig. 4(d), harmonic Hall voltage measurements were conducted with the plots showing the first and second Hall voltages for the NG sample. Figure 4(e) presents the damping-like field H_{DL} per current density for different samples. The damping-like efficiency is $1.51 \text{ Oe}/(10^9 \text{ A/m}^2)$ for the NG sample and $0.77 \text{ Oe}/(10^9 \text{ A/m}^2)$ for the PG sample. The SOT efficiency ξ_{DL} follows a similar trend, and it is defined as $\xi_{DL} = (2e\mu_0/\hbar)M_s t(H_{DL}/J_c)$. The higher SOT efficiency observed in the NG sample is attributed to the bulk Rashba effective field.¹⁹ The Hamiltonian of Rashba interaction is expressed as $H_R = \alpha_R/\hbar(\mathbf{E}_R \times \mathbf{P}) \cdot \boldsymbol{\sigma}$, which gives the bulk Rashba effective field as $\alpha_R/\hbar(\mathbf{E}_R \times \mathbf{P})$.^{19,20} Here, α_R is the Rashba parameter, $\boldsymbol{\sigma}$ represents the spin polarization vector, \mathbf{P} is the electron momentum, and \mathbf{E}_R denotes the built-in Rashba field along the direction of the spatial inversion symmetry breaking. The direction of the effective Rashba field is given by $\mathbf{E}_R \times \mathbf{P}$. For samples with NG and PG gradient directions, the \mathbf{E}_R vector points in opposite directions along the z -gradient

direction. When an electrical current flows along the $+x$ direction (with electrons flowing $-x$, $\mathbf{P} \parallel -x$), the polarized spin current associated with the Rashba effect shows the opposite y direction for the NG and PG samples, which cooperates or competes with SHE-induced polarized spin current. Consequently, the total spin polarization $\boldsymbol{\sigma}$ is given by $\boldsymbol{\sigma}_{SHE} + \boldsymbol{\sigma}_R$ in the NG sample and $\boldsymbol{\sigma}_{SHE} - \boldsymbol{\sigma}_R$ in the PG sample, which results in an increase or decrease in the SOT efficiency under the same applied electrical current. Compared to the control sample, an enhanced spin polarization in the NG sample results in a larger ξ_{DL} , whereas a reduced spin polarization in the PG sample leads to a smaller ξ_{DL} .

Previous studies on CoTb ferrimagnetic multilayers have demonstrated that a magnetization gradient can induce an effective out-of-plane field. More recent work has further revealed the presence of the OOP-SOT, attributed to broken spin conservation.^{14,19,23} To investigate this, loop-shifting measurements were carried out to probe the OOP effective field. As presented in Figs. 5(a)–5(c), experiments were conducted to measure the current-induced magnetization switching shift in the NG, PG, and (Co/Ho)₅ samples. For the NG sample, applying positive and negative currents, the loop shifts to the left and right, respectively. It indicates that a positive effective OOP magnetic field is generated by the positive current. However, for the PG sample, applying positive and negative currents causes the loop to shift right and

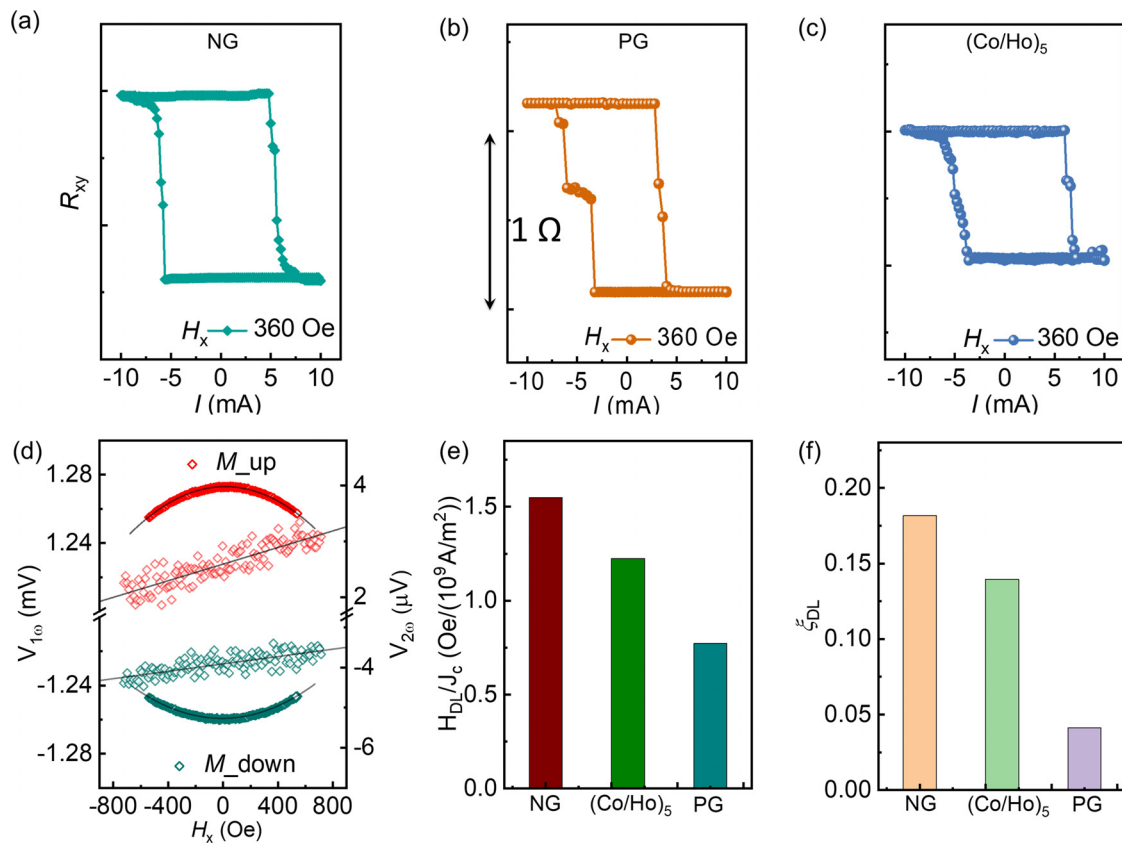


FIG. 4. Characterization of SOT efficiency. (a)–(c) Magnetization switching driven by current for the NG, PG, and (Co/Ho)₅ samples. (d) Harmonic Hall voltage signal for the NG sample. (e) Damping-like field efficiency and (f) SOT efficiency comparison for the NG, PG, and (Co/Ho)₅ samples.

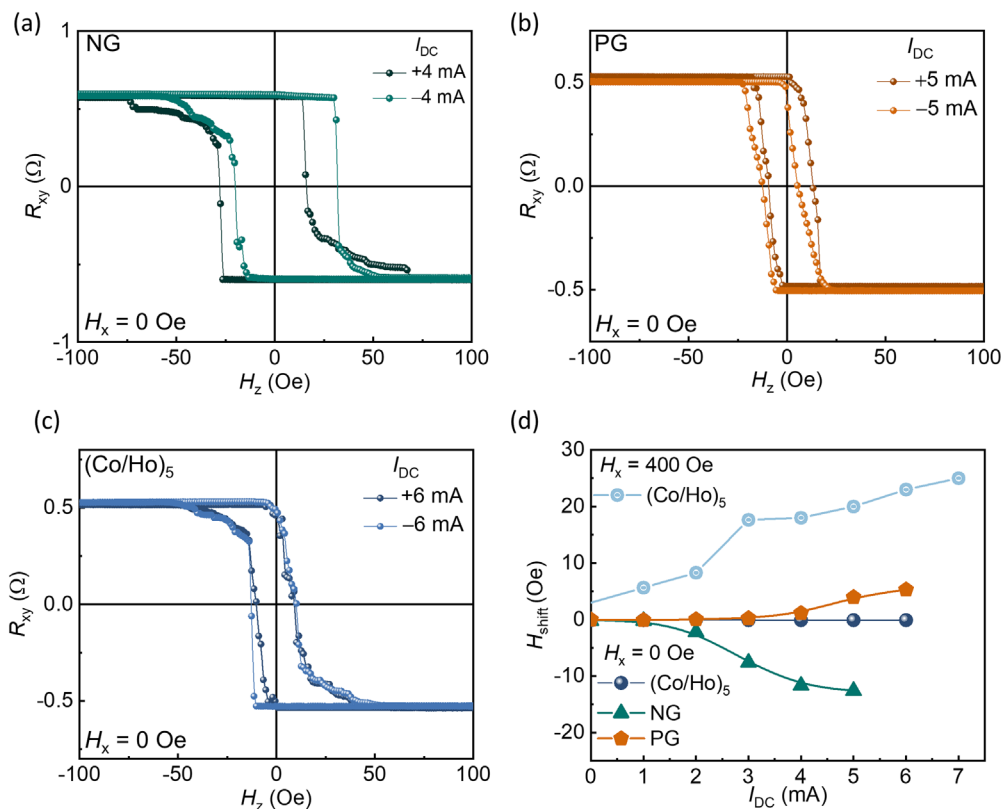


FIG. 5. Estimation of the out-of-plane effective field. (a)–(c) Loop shift measurements for the NG, PG, and $(Co/Ho)_5$ samples without in-plane magnetic field. (d) Summarized H_{shift} with I_{DC} at $H_x = 0$ Oe for the NG, PG, and $(Co/Ho)_5$ samples. The green dot shows H_{shift} for the $(Co/Ho)_5$ sample in the presence of an in-plane field of 400 Oe.

left, respectively. The effective OOP magnetic field is in the opposite direction. For the control sample $(Co/Ho)_5$, it does not display any shifting without an in-plane magnetic field, as presented in Fig. 5(c). Figure 5(d) summarizes the shift field H_{shift} generated in the NG and PG samples under $H_x = 0$ Oe. Here, H_{shift} is defined as the center shifting of the loops. When applying an in-plane magnetic field, the shifting has been observed in the $(Co/Ho)_5$ sample, as shown in Fig. 5(d), which indicates the main spin torque generated from the heavy metal Pt layer. By tuning the gradient directions, bidirectional OOP polarization has been observed, and the OOP effective field is estimated to be around $+0.7$ and -2.5 Oe/mA for the positive and negative gradient samples, respectively. However, despite the presence of an OOP effective field induced by OOP spin polarization, the magnetization switching in the Co/Ho multilayers still relies on the mechanism of domain wall nucleation and propagation. The measured OOP effective field is relatively low; hence, it is insufficient to nucleate domain walls for switching. Achieving reliable field-free switching requires further optimization of the Co/Ho gradient properties to enhance the OOP effective field and strengthen the gradient DMI contribution.

In conclusion, we demonstrated the utilization of a vertical magnetization gradient structure to achieve large charge-to-spin conversion and bidirectional OOP-SOT. This vertical gradient structure, featuring varying M_s , is engineered by alternating layers of ferromagnetic Co and rare-earth Ho, exploiting the antiferromagnetic coupling between Co and Ho layers. The bidirectional OOP-SOT associated

with gradient directions has been observed, resulting from the broken symmetry in spin current reflection and transmission in Co/Ho layers with opposite M_s gradient. Moreover, with the negative M_s gradient, the spin polarization has been enhanced, leading to improved SOT efficiency. The results presented here offer a promising approach for developing efficient, purely current-driven spin-based storage and logic devices by leveraging magnetization gradients.

This work was supported by MOE Tier 1 Grant (No. RG76/23).

AUTHOR DECLARATIONS

Conflict of Interest

The authors have no conflicts to disclose.

Author Contributions

Tianli Jin: Conceptualization (equal); Data curation (equal); Formal analysis (equal); Investigation (equal); Methodology (equal); Resources (equal); Supervision (equal); Writing – original draft (equal); Writing – review & editing (equal). **Yuliang Zhu:** Methodology (equal); Writing – review & editing (equal). **Shaomin Li:** Investigation (equal); Methodology (equal); Writing – review & editing (equal). **Bo Zhang:** Investigation (supporting); Methodology (supporting); Writing – review & editing (supporting). **Funan Tan:** Investigation (supporting); Methodology (supporting); Writing – review & editing (supporting).

Gerard Joseph Lim: Writing – review & editing (supporting). **Jiangwei Cao:** Writing – review & editing (supporting). **Kaiming Cai:** Data curation (equal); Investigation (equal); Writing – original draft (supporting); Writing – review & editing (supporting). **Wen Siang Lew:** Funding acquisition (equal); Supervision (equal); Writing – original draft (equal); Writing – review & editing (equal).

DATA AVAILABILITY

The data that support the findings of this study are available from the corresponding authors upon reasonable request.

REFERENCES

- ¹S. Bhatti, R. Sbiaa, A. Hirohata, H. Ohno, S. Fukami, and S. N. Piramanayagam, *Mater. Today* **20**(9), 530–548 (2017).
- ²Q. M. Shao, P. Li, L. Q. Liu, H. Yang, S. Fukami, A. Razavi, H. Wu, K. Wang, F. Freimuth, Y. Mokrousov, M. D. Stiles, S. Emori, A. Hoffmann, J. Åkerman, K. Roy, J. P. Wang, S. H. Yang, K. Garello, and W. Zhang, *IEEE Trans. Magn.* **57**(7), 800439 (2021).
- ³B. Dieny and M. Chshiev, *Rev. Mod. Phys.* **89**(2), 025008 (2017).
- ⁴L. Q. Liu, C. F. Pai, Y. Li, H. W. Tseng, D. C. Ralph, and R. A. Buhrman, *Science* **336**(6081), 555–558 (2012).
- ⁵S. Fukami, T. Anekawa, C. Zhang, and H. Ohno, *Nat. Nanotechnol.* **11**, 621 (2016).
- ⁶L. Liu, C. H. Zhou, X. Y. Shu, C. J. Li, T. Y. Zhao, W. N. Lin, J. Y. Deng, Q. D. Xie, S. H. Chen, J. Zhou, R. Guo, H. Wang, J. H. Yu, S. Shi, P. Yang, S. Pennycook, A. Manchon, and J. S. Chen, *Nat. Nanotechnol.* **16**, 277 (2021).
- ⁷Q. D. Xie, W. N. Lin, S. Sarkar, X. Y. Shu, S. H. Chen, L. Liu, T. Y. Zhao, C. H. Zhou, H. Wang, J. Zhou, S. Gradecak, and J. S. Chen, *APL Mater.* **9**, 051114 (2021).
- ⁸I. H. Kao, R. Muzzio, H. T. Zhang, M. L. Zhu, J. Gobbo, S. Yuan, D. Weber, R. Rao, J. H. Li, J. H. Edgar, J. E. Goldberger, J. Q. Yan, D. G. Mandrus, J. Hwang, R. Cheng, J. Katoh, and S. Singh, *Nat. Mater.* **21**, 1029 (2022).
- ⁹Y. K. Liu, G. Y. Shi, D. Kumar, T. Kim, S. Y. Shi, D. S. Yang, J. T. Zhang, C. H. Zhang, F. Wang, S. H. Yang, Y. C. Pu, P. Yu, K. M. Cai, and H. Y. S. Yang, *Nat. Electron.* **6**, 732 (2023).
- ¹⁰M. X. Wang, J. Zhou, X. G. Xu, T. Z. Zhang, Z. Q. Zhu, Z. X. Guo, Y. B. Deng, M. Yang, K. K. Meng, B. He, J. L. Li, G. Q. Yu, T. Zhu, A. Li, X. D. Han, and Y. Jiang, *Nat. Commun.* **14**, 2871 (2023).
- ¹¹D. C. Mahendra, D. F. Shao, V. D. H. Hou, A. Vailionis, P. Quarterman, A. Habiboglu, M. B. Venuti, F. Xue, Y. L. Huang, C. M. Lee, M. Miura, B. Kirby, C. Bi, X. Li, Y. Deng, S. J. Lin, W. Tsai, S. Eley, W. G. Wang, J. A. Borchers, E. Y. Tsymbal, and S. X. Wang, *Nat. Mater.* **22**, 591–598 (2023).
- ¹²B. Jinnai, C. Zhang, A. Kurenkov, M. Bersweiler, H. Sato, S. Fukami, and H. Ohno, *Appl. Phys. Lett.* **111**, 102402 (2017).
- ¹³L. Chen, K. Zhang, B. Li, B. Hong, W. T. Huang, Y. He, X. Q. Feng, Z. Z. Zhang, K. L. Lin, W. S. Zhao, and Y. Zhang, *Adv. Funct. Mater.* **34**, 2308823 (2024).
- ¹⁴Z. Y. Zheng, Y. Zhang, V. Lopez, L. Sánchez-Tejerina, J. C. Shi, X. Q. Feng, L. Chen, Z. L. Wang, Z. Z. Zhang, K. Zhang, B. Hong, Y. Xu, Y. G. Zhang, M. Carpentieri, A. Fert, G. Finocchio, W. S. Zhao, and P. K. Amiri, *Nat. Commun.* **12**, 4555 (2021).
- ¹⁵S. M. Li, H. Y. Poh, T. L. Jin, F. N. Tan, S. Wu, K. M. Shen, Y. F. Jiang, and W. S. Lew, *Appl. Phys. Lett.* **123**, 233502 (2023).
- ¹⁶L. Liu, Y. H. Song, X. T. Zhao, W. Liu, and Z. D. Zhang, *Adv. Funct. Mater.* **32**, 2200328 (2022).
- ¹⁷T. L. Jin, W. C. Law, D. Kumar, F. L. Luo, Q. Y. Wong, G. J. Lim, X. Wang, W. S. Lew, and S. N. Piramanayagam, *APL Mater.* **8**, 111111 (2020).
- ¹⁸H. Wu, J. Nance, S. A. Razavi, D. Lujan, B. Q. Dai, Y. X. Liu, H. R. He, B. S. Cui, D. Wu, K. Wong, K. Sobotkiewicz, X. Q. Li, G. P. Carman, and K. L. Wang, *Nano Lett.* **21**, 515 (2021).
- ¹⁹L. Liu, J. X. Wu, Z. X. Ye, X. T. Zhao, W. Liu, and Z. D. Zhang, *Phys. Rev. Appl.* **21**, 044013 (2024).
- ²⁰S. Wang, X. Cui, R. Xie, C. Zhang, Y. Tian, L. Bai, Q. Huang, Q. Cao, and S. Yan, *Phys. Rev. B* **107**, 094410 (2023).
- ²¹Y. Hibino, T. Taniguchi, K. Yakushiji, H. Kubota, and S. Yuasa, *Phys. Rev. B* **109**, L180409 (2024).
- ²²X. Y. Shu, L. Liu, J. Zhou, W. N. Lin, Q. D. Xie, T. Y. Zhao, C. H. Zhou, S. H. Chen, H. Wang, J. W. Chai, Y. S. Ding, W. Chen, and J. S. Chen, *Phys. Rev. Appl.* **17**, 024031 (2022).
- ²³G. Zeng, Y. Wen, C. W. Wu, C. T. Ren, D. Q. Meng, J. Zhang, W. D. Li, H. Wang, W. Luo, Y. Zhang, K. F. Dong, H. Wu, and S. H. Liang, *ACS Appl. Electron. Mater.* **5**(8), 4168–4173 (2023).